Jour. of the KGS Vol. 17, No. 3. June 2001, pp 103~110

Pore Pressure Response around a Cone Shape Penetrating Object

콘형 관입체 주변에서 발생하는 간극수압반응

Song, Chung-R.* 송 정 락

요 지

관입체 주변에서 발생하는 지반의 과잉간극수압은 그 측정위치에 따라 영향을 받는 것으로 알려져 있다. 특히 관입체의 선단과 축표면에서의 간극수압반응은 상당히 다른 것으로 알려져 있다. 본 연구에서는 지반에 대한 관입시험시 주변지반에서 발생하는 간극수압의 반응에 대하여 Louisiana State University의 시험토조를 시용하여 조사하였다. 또한 시험결과를 비등방성 수정 Cam Clay 모델을 이용한 유한요소해석과 비교하였다. 본 연구로부터 관입체 주위에서 발생하는 간극수압은 예측한 바와 같이 선단부위에서 크게 나타나고, 뒤로 갈수록 작아지는 현상을 나타내었다. 이와 같은 현상은 전단에 의하여 발생한 간극수압과 압축에 의하여 발생한 간극수압의 상호 간섭에 의한 것으로 나타났다.

Abstract

The pore pressure response of soils around a penetrating object is affected by the pore pressure measurement position. Especially it is known that the excess pore pressure response at the shaft or at the end of the penetrating shaft is different.In this paper, the pore pressure response of soils measured during the penetration test is experimentally investigated using the Louisiana State University calibration chamber test. Test results are also compared with those obtained from the finite element analysis which is based on an anisotropic modified Cam Clay model. From this study it is found that the pore pressure distribution along a penetration object is higher at the penetromerer face and lower at the penetromerer shaft as expected. This phenomenon is believed to result from the interference of shear induced pore water pressure and compression induced pore water pressure.

Keywords : Penetrometer, Pore pressure, Finite strain, Updated Lagrangian reference frame, Calibration chamber

1. Introduction

The pore pressure response of soils around a penetrating objects such as piles or penetrometers directly affects the behavior of those penetrating objects. Excess pore pressures from pile driving may be so big as to push back the pile to the surface even after the completion of pile driving. Excess pore pressure response during penetrating tests is different depending on the location of pore pressure measurements, and this behavior creates the confusion in excess pore pressure interpretation.

This study investigates the distribution of excess pore pressures along the surface of the penetrating objects. For this investigation, a penetrometer provided with 3(4) pore pressure measuring units is used, and tests are performed in the calibration chamber at Louisiana State University. Large strain elasto-plastic model provided with modified Cam-Clay model is used for theoretical approach. The investigated results showed the maximum

* Member, Director, Sambo Engrg.

excess pore pressure at the tip(face) of the model penetrometer. As the distance from tip of the model penetrometer increased, the excess pore pressure decreased. A similar trend is qualitatively expected for a penetrometer, however, it is quantitatively confirmed in this study. It is also shown that the interference of shear induced pore pressure and compression induced pore pressure do exist.

2. The Three-Piezo-Element Miniature Penetrometer

The three-piezo-element miniature penetrometer used for the tests was conceptualized at Louisiana State University and fabricated specifically for this study. A photograph of the penetrometer is shown in Fig. 1. It has a projected penetrometer area of $2cm^2$ and apex angle of 60^o. The maximum pore pressure capacity is 700 kPa. The penetrometer tip is detachable and the u_1 and u_2 porous elements are exchangeable. Therefore, the penetrometer can have two set-ups depending on porous element combinations. The possible configurations are pore pressure measurements at u_1, u_3, u_4 or at u_2, u_3, u_4. The u_1, u_2, u_3 numbering system follows the typical numbering system for the piezocone penetrometer. The u_4 is numbered last because it is behind u_3.

The pore pressure transducers are Precision Measurement Miniature Pressure Transducer Model 150F full bridge electric resistor strain gauge type sensors. For the u_1 or u_2 location, conventional leader holes are used to transmit the water pressure to the sensor (See Fig. 1.). During the saturation process, a hypodermic needle is used to inject water into the leader hole. However, for the u_3 and u_4 locations, the leader hole is not adapted, and the sensing membrane is directly placed next to the porous protective cover (See u_3 in Fig. 1.). With this configuration, the saturation process for u_3 and u_4 piezometers is substantially simplified and the volume displacement during the pore pressure measurement is minimized.

There is no friction sleeve or end resistance measuring transducers for this penetrometer. Only three pore pressure transducers are used because of the limited space in the penetrometer body. For the end resistance and friction data, separate penetration tests are carried out with another miniature penetromenter by Lim(1999). This calibration chamber test system and sample preparation procedure are essentially the same as the system expressed by Lim (2000) and Kim(2000). The essentials of the test system and sample preparation procedure are shown as follows. The details can be referred to from Lim(2000) and Kim(2000).

The specimen is essentially the combination of sand and kaolin. The grain size distribution of the kaolin and fine sand is shown in Fig. 2. Mixing is done in two large 40 gallon polyethylene tanks using a specially designed

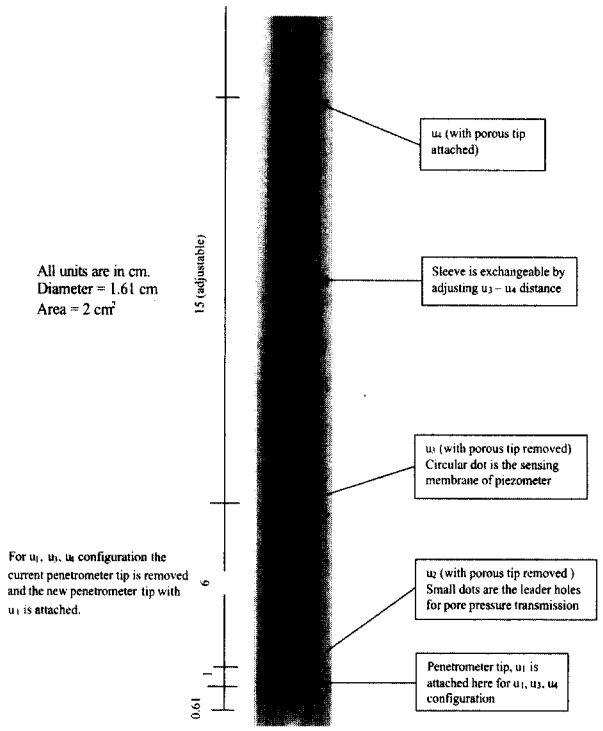

Fig. 1 The three-piezo-elements miniature penetrometer (showing u_2, u_3, u_4, configuration, units are in cm)

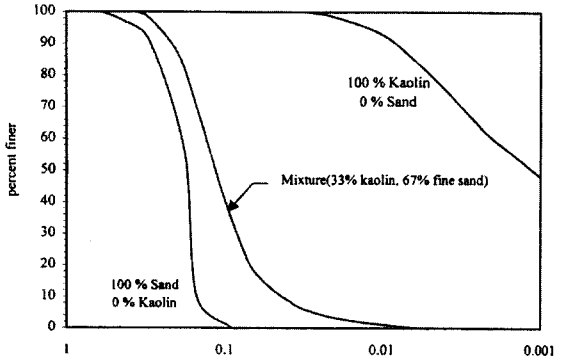

Fig. 2 Particle size distribution curves (Kurup, 1993)

Table 1. Fundamental properties of the soil mixtures

Soil	Liquid Limit (%)	Plastic Limit (%)	Plasticity Index (%)	Specific Gravity (Gs)
Kaolinite	54	28	26	2.66
Edgar Sand	.	.	.	2.67
K-33	20	14	6	

Table 2. Summary of soil parameters

Specimen	Water Content(%)	Undrained Shear Strength (kPa)	Pore Pressure Parameter, A_f	Rigidity Index, I_r	Coefficient of Consolidation ($x10^{-3}$ m^2/sec)	
					Virgin	Reload
K-33	18.56	80	.49	100	28.3	141

hand held heavy duty agitator. A mixture of 33% kaolin and 67% Edgar fine sand by weight is used to prepare the K-33 specimens. The Atterberg limits of the soil mixture are shown in Table 1. Slurry is placed very carefully inside the consolidometer with a large spoon.

A vertical consolidation stress of 138 kPa is applied to the slurry. The vertical stress is selected to obtain an initial soil specimen of sufficient strength to withstand its own weight. Higher stresses will require greater time to consolidate the specimens. Pore pressures are monitored at two different elevations and at various radial distances. At the end of the first stage of slurry consolidation, the specimen enclosed in the membrane is transferred to the calibration chamber where it is subjected to a second stage of consolidation at higher stresses. The chamber consolidation is performed with the initial back pressure (u_o) of 138 kPa to ensure saturation. After checking the B parameter for saturation, the confining pressure is adjusted for the desired pressure condition. In this work, the pressure is adjusted to σ_v'= 182 kPa (vertical), σ_h' = 75 kPa (horizontal) for K_o (=0.42) condition (OCR=1.5). The vertical stress is applied through a vertical loading jack. Horizontal stress is applied through the cell pressure. The properties of the specimen are shown in Table 2.

3. Test Procedure Using Three-Piezo-Element Miniature Penetrometer

Three penetration tests are carried out in the soil specimens. Dissipation tests are performed at the end of the penetration tests. The hydraulic system used for the penetration consists of dual pistons, double acting hydraulic jacks on a collapsible frame. The frame is mounted on top of the top lid of the chamber and allows penetration of the sample in a single stroke of 640 mm or less. Such a single stroke continuous penetration is desirable especially in saturated cohesive specimens where stress relaxation and pore pressure dissipation can occur during a pause between strokes. The penetration depth is measured using an electronic analog to digital converter depth decoding system. All tests are conducted at the standard penetration rate of 2cm/sec. Validity of the penetration rate of 2cm/sec for miniature penetrometer is discussed later. A total of three penetration tests are performed. Tests 1 and 2 are performed for the two different piezoelement configurations, the u_1, u_3, u_4 configuration and the u_2, u_3, u_4 configuration, respectively. Test 3 has the same configuration as Test 2. The main purpose is to check the repeatability of the tests.

Data acquisition is carried out both manually and automatically. The pore pressure response is recorded with digital, which is hooked up to the computer's data acquisition system. Also, the readings of the digital voltmeters are recorded by a video camera in case of data acquisition system failure. Data is taken per second. During the dissipation test, the sampling frequency is reduced to lower frequency because of the prolonged measuring time. The testing equipment set up is shown in Fig. 3. The verification of the three-Piezo-element Miniature Penetrometer is also performed. A large hose that has about the same diameter as the three-Piezo-

element Miniature Penetrometer is placed over the piezometers tips, and water pressure is applied in the rubber tube. The measured water pressures from the three-Piezo-element Miniature Penetrometer were compared and calibrated with the known water pressures of the calibration system.

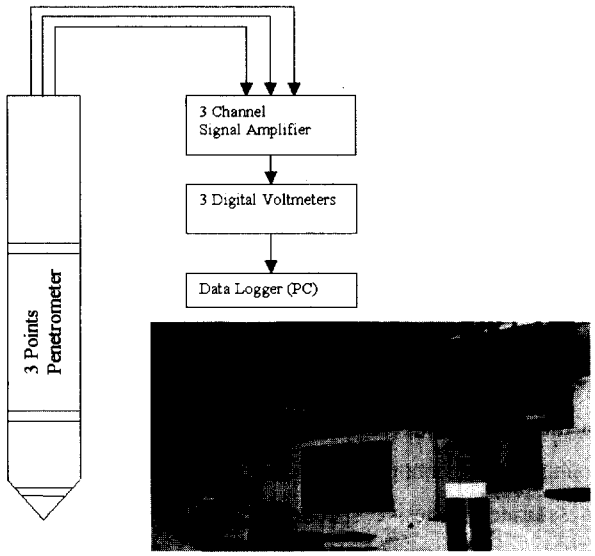

Fig. 3 Test set up

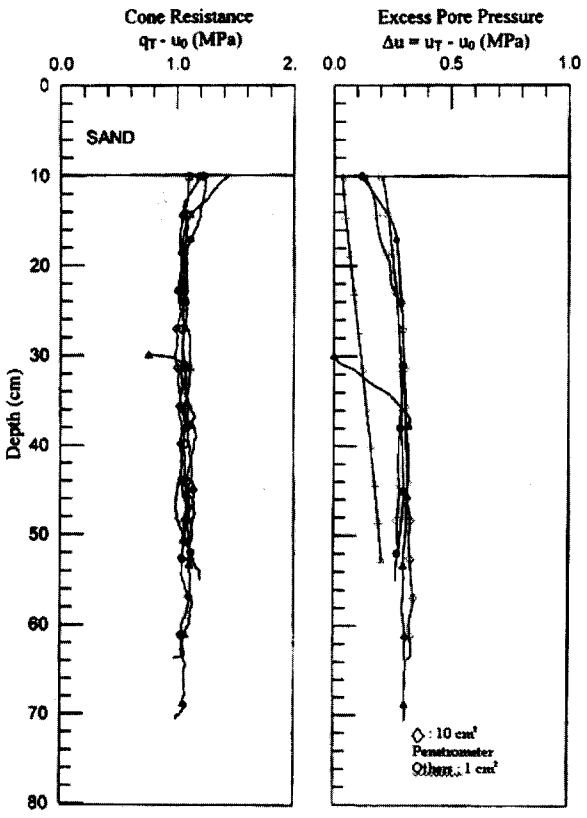

Fig. 4 Comparison of penetration results for the reference cone ($10cm^2$) and miniature cone ($1cm^2$) penetrometer (Lim, 2000)

Validity of penetration rate was carefully investigated because of the scale difference of the three points penetrometer and the (standard) reference cone penetrometer. The three points penetrometer has cross sectional area of $2cm^2$ and the reference cone has cross sectional area of $10cm^2$. Regarding this scale difference, the increase of penetration speed for the three points penetrometer was considered.

Comprehensive comparison of penetration speed effects for cone penetrometer by Lunne et al. (1997) showed inconsistent trend. Also, the results of Roy et al.(1982) showed a non-significant difference in excess pore pressure change for the penetration speed range of 3cm/sec - 240cm /sec. The test results by Lim(1999) also showed a nonsignificant difference in excess pore pressure between a reference penetrometer and a miniature penetrometer with cross sectional area of $1cm^2$ as shown in Fig. 4. Consequently, the penetration speed of 2cm/sec was adopted in this test. Therefore, the effects of penetration speed is excluded from the scope of this study.

4. Results

Test results are shown in Fig. 5. Fig. 5-a is the combined representative results for the u_1, u_2, u_3, and u_4 locations. Pore pressure response for the u_1 location shows typical results obtained in the penetration tests. The steady state pore pressure is obtained about two seconds after the start of penetration. u_2 also shows a similar response. The absolute magnitude of u_2 is a little smaller than u_1 and this is similar to other experimental results.

The results of the pore pressure for u_3 and u_4 in Fig. 5-a show a substantial initial drop and an increase up to the steady state condition. It is an unexpected behavior. However, careful evaluation of the pore pressure at the u_3 and u_4 locations presents very meaningful phenomena. One can note that the distance from the penetrometer tip to the u_3 and u_4 locations are 7 cm and 22 cm, respectively. In Fig. 5-a, one can note that the steady state

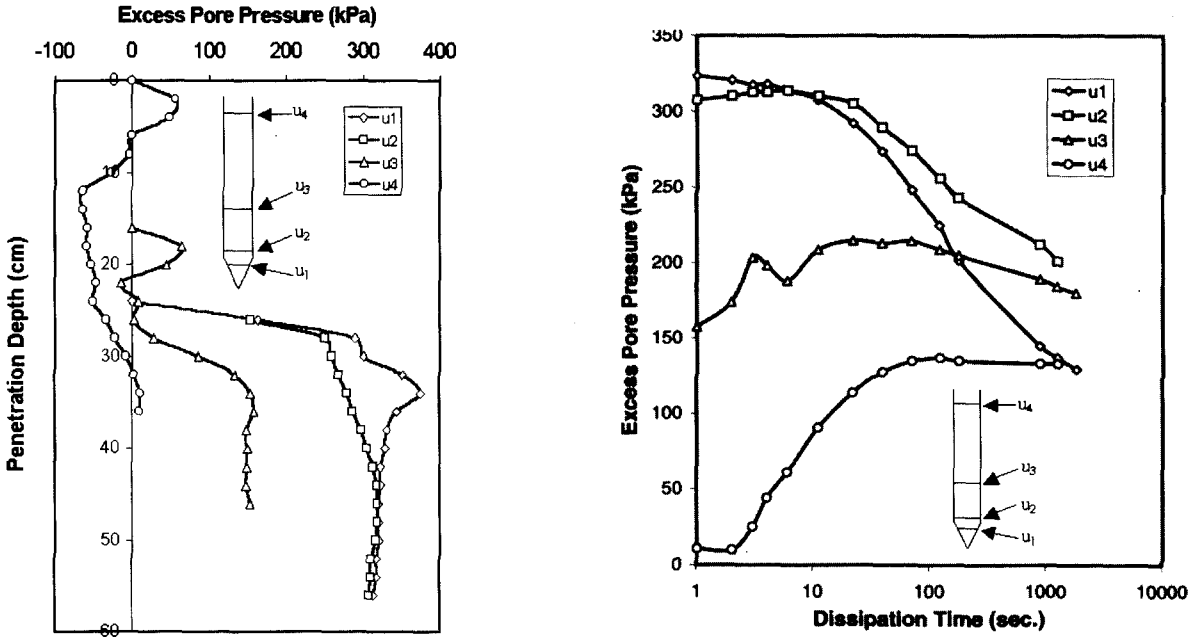

(a) Combined penetration test results for u_1, u_2, u_3, and u_4 location

(b) Dissipation curves of u_1, u_2, u_3, and u_4 locations

Fig. 5 Measure pore pressure

condition for the u_1 is obtained in a relatively short time. This response is similar to the u_1 response of other researches (Kurup 1993, Lunne et al. 1997). The rapid achievement of the steady state represents the rapid achievement of the new(dynamic) equilibrium condition. The steady state represents constant boundary conditions such as stabilized flow and stress-strain conditions. The initial boundary conditions of u_1 change to the initiation of the penetration.

New boundary conditions are then developed. Once these new boundary conditions are developed for u_1, they reach the stable condition in a very short time. The response of u_2 is slightly different from that of u_1. u_2 shows a slight initial hesitation and that is followed by a similar trend as u_1. This initial hesitation is more clearly observed in the response of u_3. This initial hesitation period is much longer than that of u_2. u_3 also shows two steady state conditions. The first steady state is in the initial hesitation period and the second steady state is in the second stabilized period. These two steady states are even more prominent in the u_4.

Here, one needs to focus on the steady state or equilibrium mechanism around the penetrometer tip and shaft. u_1 is at the penetrometer face. Penetration will alter the initial boundary conditions such as the flow and stress-strain conditions. Subsequently u_1 attains new boundary conditions. Initially u_1 is subjected to no flow and at rest stress condition. After the start of penetration, u_1 is subjected to a transient flow with compression and shear stress condition. These transient conditions for u_1 are the new boundary conditions for u_1, and they last as long as the penetration continues. u_2, u_3, and u_4 are located at the penetrometer shaft. Once penetration starts, these points are subjected to the transient flow and primarily shearing condition. For example, these shearing boundary conditions for u_3 will be maintained until u_3 meets the initial depth of u_1. Therefore u_3 can have an initial hesitation period or stage one steady state period. However when u_3 penetrates to the previous location of u_1, u_3 then will enter into the disturbed zone caused by u_1(penetrometer face). At the disturbed zone, the flow and stress-strain conditions are different. Therefore, u_3 will undergo new equilibrium conditions. Especially in the case of the pore pressure response of normally consolidated soils, the disturbed zone caused by u_1 has positive excess pore pressure. This will show increased pore

pressure as u_3 passes the previous location of u_1.

u_2 is located at the penetrometer shaft, however, it is very close to u_1. Pore pressure response time difference between u_1 and u_2 is less than one second. This is the reason why u_2 has a very short initial hesitation. u_3 and u_4 are relatively far from u_1 compared to u_2, and they show clearer initial hesitation or first stage steady state.

Independently from this study, Elsworth(1993) predicted the time to reach 95% of the steady state penetration generated pore pressure based on the dislocation scheme. For the case of a penetration speed of 2cm/sec and a coefficient of consolidation, $28.3 \times 10^{-3} m^2/sec$, the time required to reach 95% of steady state penetration generated pore pressure is about 0.5 seconds for the penetrometer tip. That number is 10 seconds for the penetrometer shaft at the location ten times the radius of the penetrometer behind the penetrometer face. From Elsworth(1993), one notes that the minimum penetration depth for achieving the steady state condition is quite short for the case of the penetrometer tip. However, that distance increases substantially for the penetrometer shaft. Elsworth's findings do not exactly agree with the experimental results in this study, however, they show conceptual agreement with the test results in this study.

From this discussion, one can see that for a better analysis of the penetrometer penetration test, a substantial amount of penetration is required especially for the analysis of the friction on the penetrometer shaft. Fig. 5-a also shows the steady state pore pressure distribution which is high at the penetrometer tip and low (gradual decrease) along the penetrometer shaft. This trend agrees well with Levadoux and Baligh's(1986) experimental results, and Whittle and Aubeny's(1991) and Elsworth's (1993) theoretical results. Fig. 5-b shows the dissipation test results carried out at the end of the penetration for all four piezometer locations. u_1 shows the typical dissipation curve. The computed hydraulic conductivity from u_1 dissipation curve is about $2 \times 10^{-8} m/sec$ (t50 method of Robertson et al.(1992). Considering the fact that the measured hydraulic conductivity value in the laboratory (constant head hydraulic conductivity tests for the triaxial specimen with a confining pressure having the same magnitude as the effective vertical overburden pressure of the specimen) is $2.1 \times 10^{-8} m/sec$, one concludes that the computed hydraulic conductivity is in very good agreement with the laboratory test results. However, u_2 shows some deviation from the standard back-bone shape of the dissipation curve. u_3 and u_4 show large deviation from the standard dissipation curve and may not be used for the computation of the soil hydraulic conductivity or the consolidation coefficient.

The following observations are made in reference to Fig. 5-b with respect to the mechanism of the unstable pore pressure dissipation curve. For the u_1 location, a faster pore pressure dissipation is observed, which may indicate a spherical dissipation. The spherical dissipation is proportional to r^3 while cylindrical dissipation is proportional to r^2, where r is the radius of the penetrometer. For the u_2, u_3, and u_4 locations, the dissipation condition may be assumed to be of a cylindrical condition (horizontal drainage). However, the initial pore pressure is very unstable and far from the standard back-bone shape. Through the previously discussed two stage equilibrium case one observes that small (even negative) pore pressure is generated at the penetrometer shaft, and it approaches the state-one steady state until it enters a new boundary. After the penetration of the penetrometer stops, an interaction starts between the penetrometer tip generated pore pressure and the penetrometer shaft generated pore pressure in order to attain pore pressure equalization. The high pore pressure from the far field flows into the near field of the penetrometer shaft. Therefore, it shows an initial increase in the pore pressure response for the u_2, u_3 and u_4 as indicated in Fig. 5-b. Based on the above discussion, one can now explain the response of the u_1, u_2, u_3 and u_4. In Fig. 5-a and Fig. 5-b, however, the dissipation curves for the penetrometer shaft locations (u_2, u_3, u_4) deviate substantially from the standard back bone shape and are difficult to use for the evaluation of the coefficient of consolidation or soil hydraulic conductivity. The response of u_2 is somewhat close to u_1. However, the above discussed pore pressure interaction is still there.

The proposed method, which does not utilize the dissipation curve, is presented in the next section.

5. Numerical Simulation

The calibration chamber test results are compared with numerical simulation results. Numerical simulation is carried out based on the Prevost (1980) coupled theory of mixtures and an anisotropic modified Cam Clay model (Voyiadjis and Song, 2000). An updated Lagrangian reference frame is used for large strain elasto-plasticity. Numerical simulation results are shown in Fig. 6. Fig. 6 shows a steady state pore pressure at the penetrometer tip. Fig. 6 shows a high excess pore pressure at the tip (face) and smaller excess pore pressure at the penetrometer shaft. Fig. 6 does not show the pore pressure response for longer distance from the tip. This is because the numerical simulation was performed for penetration distance 2.5cm, and penetration length in Fig. 5-a is more than 50cm (Numerical simulation for 50cm penetration is not possible.). The numerical simulation of steady state penetration for the penetrometer shaft is not quite possible at this moment, therefore, the pore pressure response at the penetrometer shaft is not realistic.

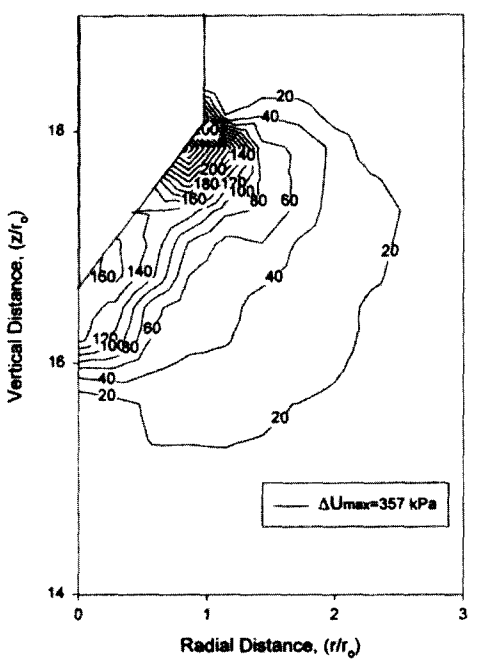

Fig. 6 Analytical prediction of excess pore pressure distribution around a penetrating object

However, one can know that the trend of Fig. 6 is similar to that of Fig. 5-a. Therefore one can see that experimental results in Fig.5-a and analytical results in Fig. 6 agree fairly well.

6. Conclusions

New experimental investigation of the penetration induced excess pore pressure is carried out in this study. A specially designed three-piezo-element penetrometer is designed and tested in the Louisiana State University Calibration Chamber. The large strain coupled theory of mixtures formulation using an updated Lagrangian reference frame is adopted for this work.

From this study, the following conclusions are made:

1) The generated pore pressure at the penetrometer tip is mainly due to the compressive stress, and is usually positive.

2) The generated pore pressure at the penetrometer shaft is combination of shear induced pore pressure and compression induced pore pressure.

3) Sometimes, the shear induced pore pressure is negative, and the combined pore pressure can be negative or very small.

4) Due to this interference of shear induced pore pressure and compression induced pore pressure, the dissipation of pore pressure does not follow standard back-bone type dissipation curve when the pore pressure measurement position is not at the tip.

5) The steady state for the penetrometer shaft is obtained in two stages because of the change in boundary conditions while that of the penetrometer tip is obtained in one stage because of the constant boundary conditions. Due to this phenomenon, the dissipation curve of the penetrometer shaft (especially u_3, and u_4) deviates largely from the standard back-bone shape curve. However, at the penetrometer tip position, the interference of pore pressure is minimal, the dissipation curve follows standard back-bone shape curve.

References

1. Elsworth, D. (1993), "Analysis of Piezocone Dissipation Data Using Dislocation Methods," J. of GE. ASCE, Vol.119, No.10, pp.1601-1623
2. Kim, D.K. (2000), "A Study on the Model Parameters of the Anisotropic Elastoplastic-Viscoplastic Bounding Surface Model for Cohesive Soils," J. of Korean Geotechnical Society, Vol.16, No.3, pp.67-76
3. Kurup, P.(1993), *Calibration chamber studies of miniature piezocone penetration tests in cohesive soil specimen*, Ph. D. Dissertation, Louisiana State University, Baton Rouge, LA. 70808
4. Levadoux, J.N. and Baligh, M.M. (1986), "Consolidation after Undrained Piezocone Penetrometer, I: Prediction," J. of GE. ASCE, Vol.112, No.7, pp.707-725
5. Lim, B.S. (2000), "Determination of Consolidation Characteristics in Fine Soils Evaluated By Cone Penetration Test," Proceedings of Soft Soil Committee of Korean Geotechnical Society 2000 Spring, pp.42-58
6. Lim, B.S. (1999), *Determination of Consolidation Characteristics in Fine Grained Soils Evaluated by Piezo Cone Tests*, Ph. D. Dissertation, Louisiana State University, Baton Rouge, LA 70808
7. Lunne, T., Robertson, P.K., and Poweli, J.J.M.(1997), *Cone Penetration Testing*, Blakie Academic & Professional, pp.127-132
8. Prevost, J.H. (1980), "Mechanics of continuous porous media," International Journal of Engineering Science, Vol. 18, 787-800
9. Robertson, P.K., Sully, J.P., Woeller, D.J., Lunne, T., Powell, J.J.M., and Gillespie, D.G. (1992), "Estimating coefficient of consolidation from piezocone tests," Canadian Geotechnical Journal, Vol. 29, No.4, pp.551-557
10. Roy, M., Trembley, M., Tavenas, F., and LaRochelle, P. (1982), "Development of Pore Pressure in Quasi-Static Penetration Tests in Sensitive Clay," Canadian Geotechnical Journal, Vol.19, No.2, pp.124-138
11. Voyiadjis, G.Z. and Song, C.R. (2000), "Finite Strain Anisotropic Modified Cam Clay Model with Plastic Spin I: Theory," J. of EM Div. ASCE, Vol.126, No.10, pp.1012-1019
12. Whittle, A.J. and Aubeny, C.P. (1991), "Pore pressure fields around piezocone penetrometers installed in clay," Proceedings of the 7th International Conference on Computer Methods and Advances in Geomechanics, Cairns, pp.285-90

(received on May 10, 2001)